Progress In Electromagnetics Research M, Vol. 97, 13–24, 2020

Microwave Imaging Solutions for Medical Imaging Using Re-Weighted Basic Pursuit Algorithm

Thathamkulam A. Anjit[1, *], Ria Benny[1], Philip Cherian[2], and Palayyan Mythili[1]

Abstract—This paper describes an innovative technique for the quantitative reconstruction of the dielectric and conductivity distribution of objects in a microwave tomography framework using sparse data. The proposed method tries to extract information about the size, shape, localisation, and dielectric distribution of various inclusions within the object under study using an iterative reconstruction methodology in the sparse domain. The proposed algorithm combines the Distorted Born Iteration method (DBIM) and a convex optimization technique for solving the inverse ill-posed problem. The Re-weighted Basis Pursuit (RwBP) algorithm is chosen as the convex optimization technique in this work. The performance of the proposed algorithm has been compared with the TV-norm method, and the results obtained are highly encouraging. The proposed method produces a significant reduction in the reconstruction error as compared to the TV norm method with an error value of 0.083 as against 0.32 in the case of TV norm in the presence of 25 dB noise. By accurately preserving the edges of the inclusions, the proposed technique is found to provide an overall improvement in the reconstruction in terms of tissue differentiation (permittivity and conductivity), dimensions of inclusions, resolution, shape, size, and coordinate localisation of inclusions. The proposed algorithm converges within 10–12 iterations as compared to other complex imaging algorithms available in the literature. Further, this proposed technique is validated using experimental data from an actual breast imaging setup. The three inclusions of 10 mm, 6 mm, and 3 mm have been localised with errors of 0.052, 0.04, and 0.09, respectively. The results obtained from the real-time data show the applicability and feasibility of the proposed algorithm in breast tumor imaging application.

1. INTRODUCTION

Microwave Imaging (MWI) has proven its potential utility and effectiveness for a wide range of applications. MWI for medical applications has promoted immense enthusiasm among the researchers continuously. Conventional medical imaging systems currently used for diagnosis have many disadvantages. X-ray mammography and CT scans cannot be used routinely on patients due to radiation hazards and a high probability of false positives. Ultrasound and PET scans suffer from poor resolution and involve procedures that cause discomfort for the patients. The diagnosis of malignant tissue or tumorous growth using microwave imaging is thus a viable alternative with attributes like safety, non-ionizing nature, reasonable penetration into the human tissue, and affordability. The key to microwave imaging lies in the difference in the dielectric values between the normal tissues and malignant growths. The same technique can be used for the detection of myocardial infarction based on the differences in dielectric properties between normal and infarcted tissues in microwave based cardiac imaging [1]. The MWI process to detect the dielectric value differences (contrast function) proceeds in two steps, namely, forward problem and inverse problem. The forward problem involves the illumination of the object under study and the collection of the scattered waves. An estimate of the spatial distribution

Received 30 June 2020, Accepted 4 September 2020, Scheduled 25 September 2020
* Corresponding author: Thathamkulam Agamanan Anjit (taanjit@yahoo.in).
[1] Cochin University of Science and Technology, Cochin, Kerala, India. [2] College of Engineering, Chengannur, Kerala, India.

of the dielectric properties of the object is obtained from the measured scattered fields, by solving the corresponding electromagnetic Inverse Scattering Problem (ISP) [2–4].

The formulation of ISP presents several theoretical and practical difficulties. Solving the contrast function from the ISP is done by evaluating the Electric Field Integral Equation (EFIE). These EFIE equations are nonlinear with two sets of unknown quantities (a) dielectric profile and (b) the total electric field inside a scattering object. This nonlinearity leads to a large number of numerical solutions [5] due to three major limitations (a) presence of evanescent waves, (b) local minima, (c) sensitivity of the inverse problem to noise [6]. Since the evanescent waves produced in the region under study do not reach the receiver location, fine-grained details will be lost in the inversion process. The remaining two limitations in the case of an under-determined problem can be avoided by increasing the number of transmitting and receiving antennas and by employing a suitable regularization technique in addition to the actual inversion algorithm.

The commonly used approach to solve the inverse problem is to rely on iterative inversion algorithms based on approximations like Born iteration method (BIM) or Distorted Born iterative methods (DBIM), which solve the linear version of the nonlinear problem to some extent [7]. By using BIM or DBIM, the contrast profile can be reconstructed to a resolution of one tenth of the wavelength [8]. If the object to be imaged is more complex, the resolution that can be achieved will be reduced to half of the wavelength [9]. Since the resolution is proportional to the number of unknowns, the constraints on the number of unknowns to be estimated from a set of under-determined equations make it a challenging problem. To overcome these issues and challenges, various regularization and optimisation methods have been proposed by researchers to solve the ill-posed inverse problem. Stochastic techniques like Genetic Algorithm, Particle Swarm Optimization, differential annealing, Ant Colony Optimization, etc. have been successfully applied to optimise the solution to the inverse scattering problem [10]. However, due to the increased computational complexity posed by these methods, they are less preferred by researchers. In the case of deterministic regularisation methods like Singular Value Decomposition (SVD), Conjugate Gradient Least Squares (CGLS), Tikhonov method, etc., the inverse problem is modeled as an objective function, and it is subjected to some form of minimization technique [11]. However, when the imaging domain has sharp variations and discontinuities, these regularization methods will produce extra smoothness instead of sharp changes and eventually become inefficient.

To overcome the above-mentioned limitations, compressive sensing (CS) technique was introduced into the MWI domain in 2008 [12]. CS is a popular technique in signal processing which is able to reconstruct sparse or compressible signals exactly from a limited number of measurements, by solving the optimization problem accurately. CS theory can be applied to those cases where the problem under consideration is linear as well as when the unknown can be represented with only a few non-zero coefficients in a given basis. Microwave imaging could in principle take significant advantage from CS techniques, because of its ability to solve the under-determined set of equations using sparsity. Due to the advantages of the CS techniques, it is currently widely used in conventional medical imaging field such as MRI [13], CT [14], and PET [15]. It is a promising technique which can reduce the cost of data acquisition and storage requirement.

Various algorithms have been proposed in the CS framework for MWI. One such method is the Iterative Shrinkage Thresholding Algorithm (ISTA) which is gradient-based, where each iteration involves matrix-vector multiplication followed by a shrinkage/soft-threshold step. However, they have been recognized to produce a slow convergence [16]. Accelerated versions of ISTA like TWo-step IST (TWIST), NESTA (Nesterov's ISTA), Fast ISTA (FISTA), etc. are used to solve ISP with a faster rate of convergence. Methods such as the Iterative Method with Adaptive Thresholding for Compressed Sensing (IMATCS) in conjugation with the non-decimated wavelet transform [17] and the Total variation (TV) CS [18] method (TV minimizes the integral of the gradient of the contrast function) were proposed with better performances to overcome the slow convergence rate of the basic IMATCS algorithm, mainly when there are a large number of degrees of-freedom.

The nonlinearity and ill-posedness of the electromagnetic inverse scattering problem can lead to unstable reconstructions in MWI medical applications when dense or closely located scatterers appear in the investigation region. In this paper, a two-dimensional (2D) tomographic reconstruction algorithm namely the Re-weighted Basic Pursuit algorithm that provides a robust reconstruction along with a better resolution has been proposed for medical applications. The inverse problem has been considered

in the Compressive Sensing framework, and it is reviewed under the versatility offered by a convex optimization approach. The performance of the proposed method has been validated using experimental results and compared with the results reported by Jamali et al. [19].

The paper has been organised as follows. Section 2 describes the linear approximation of the electromagnetic inverse problems along with the reconstruction algorithm under a CS framework. Section 3 elaborates the reconstruction of the dielectric profile and its performance against noise. The experimental setup used for imaging has been described, and the results obtained by reconstructing the collected scattered data using the proposed method have been discussed as well. Section 4 concludes the paper.

2. IMAGING ALGORITHM UNDER COMPRESSIVE SENSING FRAMEWORK

Microwave imaging is broadly classified into two categories, namely qualitative and quantitative. The qualitative approach aims at obtaining localisation information about the scatterer (object function) like shape, size, position, etc. This approach, however, is unable to retrieve the electromagnetic parameters of the scatterers. This section describes the quantitative deterministic reconstruction method, aimed to retrieve the values of the dielectric parameters of the imaging domain. This is achieved by solving the nonlinear system of equations relating the unknown dielectric properties to the measured scattered field. Section 2.1 discusses the formulation of the forward and inverse problems to obtain the quantitative dielectric profile. Section 2.2 describes the re-weighted l_1 analysis in the sparse domain to solve the inverse problem.

2.1. Linear Approximation of EM Inverse Scattering Problem with DBIM

The objective is to image the dielectric contrast profile of the scatterer under consideration from the finite number of scattered data measured around the vicinity of the object of interest. The tomographic arrangement of the transmitter and receiver antennas for MWI is shown in Fig. 1. The object under investigation is assumed to be inhomogeneous with respect to the dielectric permittivity ϵ_r and conductivity σ, which is immersed in a homogeneous background medium having a permittivity ϵ_b. For any 2D scattering problem, the complex dielectric profile varies only in the X-Y plane. The object is illuminated by a TM polarised wave whose magnetic field is transverse to the axis of the scatterer. N_t number of transmitting antennas and N_r number of receiver antennas are positioned around the object

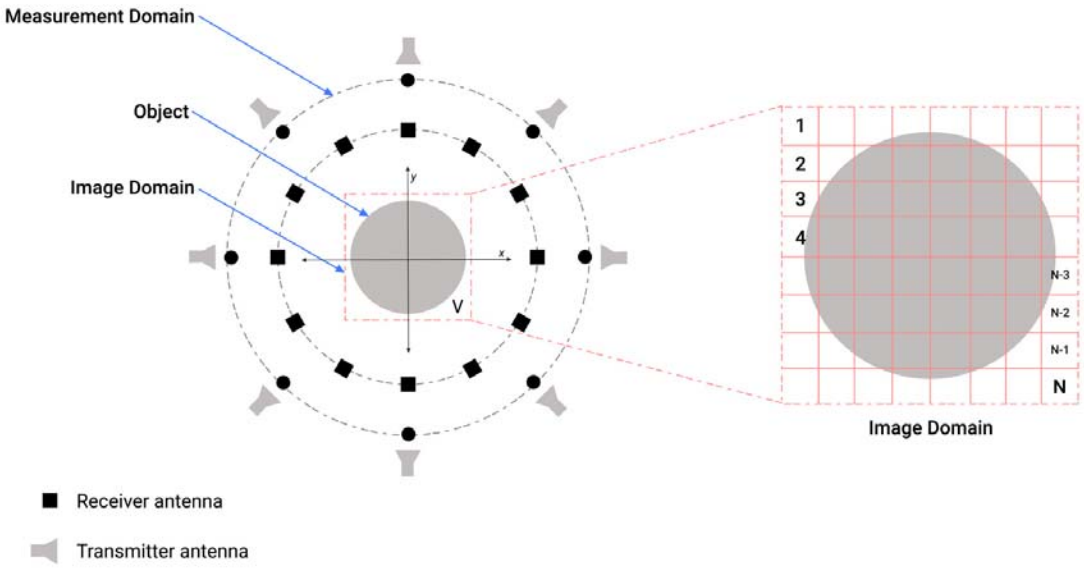

Figure 1. Tomographic arrangement of transmitter and receiver antennas.

at equal angular intervals. The entire arrangement corresponding to Fig. 1 is divided into an object domain, i.e., the area which encloses the object to be imaged and the measurement domain, where the measurements are done. The object domain is further divided into a grid of square-shaped cells, and within each cell, the total electric field and the complex permittivity are assumed to be a constant. The distance to any point inside the object domain is r and to any measurement point is r' from the origin.

The imaging procedure begins with the transmitters illuminating the object under study at multiple frequencies. The scattered fields for the given scatterer are then obtained at the receivers. This process is termed as the forward problem. The relation between the values of the scattered field and the total field at any point in the object domain is given by

$$E^{sc}(r) = E^t(r) - E^i(r) \tag{1}$$

$$= \omega^2 \mu \int_V dr' \overline{G}(r, r') \Delta\epsilon(r') E^t(r') \tag{2}$$

$$\Delta\epsilon = \frac{\epsilon(r) - \epsilon_b(r)}{\epsilon_b(r)} \tag{3}$$

where E^{sc} is the scattered Electric field, E^t the total field, and E^i the incident field. $\overline{G}(r, r')$ represents the Green's function, and $\epsilon(r)$ represents the permittivity over the object domain, V. The forward problem is well posed and is solved using the Method of Moments (MoM) technique. The electric field integral equation (EFIE) expressed in Equation (2) can be discretized and written in matrix form as

$$[E^{sc}] = [G] \left[E^t\right] [\Delta\epsilon] \tag{4}$$

After evaluating the scattered field using Equation (4), the next step is to solve the inverse problem. The dielectric profile of the object under investigation can be deduced from the measured scattered data by using the deterministic algorithms like BIM, DBIM, etc. These algorithms are used to solve the inverse scattering problem by linearizing it around a current estimate of the dielectric permittivity and then seek progressively better estimates of the dielectric profile.

However, due to the nonlinearity of the inverse scattering problem, there is a risk that the solution gets trapped in local minima. To avoid the nonlinearity, Born approximation replaces the total unknown field, $E^t(r)$, with the known incident field. This approximates the nonlinear ISP with an under-determined set of linear equations. The contrast function, $\Delta\epsilon$, is estimated from the resulting linear integral equation at each iteration of the DBIM algorithm. The DBIM algorithm alternates between the forward and inverse problems until it converges to a unique solution for the contrast function. The above ill-posed inverse problem can be represented in linear form as

$$y_{M\times 1} \approx \Phi_{M\times N} x_{N\times 1} \tag{5}$$

where y is the data vector matrix representing the measured scattered field, x the unknown contrast function, and Φ the measurement matrix which is the product of Green's function and the total field. In the case of inverse imaging, the number of unknowns N (depends upon resolution of reconstruction) is very much greater than the number of measured field values M, due to which the problem is ill-posed. The aim is to recover x from the given scattered measurement data, y. A commonly used method to solve the ill-posedness is to exploit the sparsity of the vector x. The key behind compressive sensing lies on the sparsity of the signal and the incoherence of the sensing matrix. The profile to be reconstructed is considered to be complex denoted by the vector $x \in C^N$. For the sparse transformation, an orthonormal basis $\Psi \in C^{N\times N}$ is considered, in which the decomposition vector $\alpha \in C^N$ of the profile may be defined such that $x \equiv \Psi\alpha$. The signal is said to be sparse if it contains only K non-zero coefficients in its decomposition [12], where $K \ll N$. The corresponding ill-posed inverse problem is defined as

$$y \equiv \Theta\alpha + n \quad \text{with} \quad \Theta \equiv \Phi\Psi \in C^{M\times N} \tag{6}$$

where $n \in C^M$ is the independent and identical distributed noise. Recovering α from Eq. (6) proceeds by finding the sparsest representation of α, subject to the following constraint:

$$\min_{\overline{\alpha} \in C^N} \|\overline{\alpha}\|_0 \quad \text{subjected to} \quad \|y - \Theta\overline{\alpha}\|_2 \leq \zeta \tag{7}$$

where $\|\overline{\alpha}\|_0$ counts the non-zero elements in $\overline{\alpha}$, and ζ is the upper bound of the l_2 norm on the residual noise n. The problem in Equation (7) is combinatorial, and NP-complete as the l_0 norm is discrete and

discontinuous in nature. Among many possible solutions to $\Theta\alpha = y$, the one in which the coefficients have minimum l_1 norm is selected [20, 21]. In practice, however, the signals are rarely sparse and are often corrupted by noise. The problem then changes to the reconstruction of an approximately sparse signal x from its noisy measurements. In the presence of noise, the Basic Pursuit De-noising (BPDN) or LASSO [22] is the minimization of l_1 norm of the coefficients of the signal in the sparsity basis, under a constraint on the l_2 norm of the residual noise n.

$$\min_{\overline{\alpha}\in C^N} \|\overline{\alpha}\|_1 \quad \text{subjected to} \quad \|y - \Theta\overline{\alpha}\|_2 \leq \zeta \tag{8}$$

The key difference between l_1 minimization and l_0 minimization is that l_1 depends on the magnitude of the coefficient whereas l_0 depends on the count of non-zero elements. These two techniques become equivalent when the measurement matrix satisfies a certain condition under the compressive sensing context [23, 24]. To reconcile this imbalance, a re-weighted l_1 minimization algorithm was proposed by Candés et al. to mimic the l_0 minimization behaviour. Re-weighted l_1 minimization is a suitable alternative when there is prior information regarding the signal to be recovered.

The algorithm proposed in this paper replaces the l_1 norm in Equation (8) by the weighted l_1 norm $\sum_{i=1}^{N} w_i|\bar{\alpha}|$, resulting in the formation of the re-weighted basis pursuit (RwBP) algorithm.

2.2. Object Profile Reconstruction — Re-Weighted Basis Pursuit Analysis

The reconstruction algorithm defined in Algorithm 1 [25] consists of solving a sequence of weighted l_1 minimization problems. A weighted l_1 problem is defined as

$$\min_{\overline{x}\in R^N} \|W\Psi^T\overline{x}\,\|_1 \quad \text{subjected to} \quad \|y - \Phi\overline{x}\,\|_2 \leq \epsilon \quad \text{with} \quad \overline{x} \geq 0 \tag{9}$$

where $W \in R^{D\times D}$ is a diagonal matrix with positive weights. In the case of the re-weighted approach, a sequence of weighted l_1 problems are solved, and the weights used for the next iteration are computed from the values of the current solution. By using the function $f(\gamma, x)$, the weights are updated after each iteration as

$$f(\gamma, x) \equiv \frac{\gamma}{\gamma + |x|} \tag{10}$$

where γ plays the role of stabilization parameter, and as $\gamma \to 0$ the weighted l_1 norm approaches the l_0 norm. To approximate l_0 norm by the re-weighted l_1 algorithm, a homotopic strategy [26] is adopted, which consists of solving a sequence of weighted l_1 problems using a decreasing sequence $\{\gamma^{(t)}\}$, where t represents the iteration variable.

Algorithm 1 Image Reconstruction Algorithm

Require: $y, \Phi, \beta, \epsilon, \sigma_c, N_{\max}$
Ensure: Reconstructed Profile $\widehat{x}$
1: Initialize $W^{(0)} = I, t = 1$ and $\rho = 1$
2: Compute
   $\widehat{x}^{(0)} = \triangle(y, \Phi, W^{(0)}, \epsilon)$
   $\gamma^{(0)} = \sigma_s(\Psi^T\widehat{x}^{(0)})$
3: **while** $\rho > \eta$ and $t < N_{\max}$ **do**
4: Update the Weight Matrix:
   $W_{ij}^{(t)} = f(\gamma^{(t-1)}, \widehat{\alpha}_i^{(t-1)})\delta_{i,j}$, for $i, j = 1, ..., D$ with $\widehat{\alpha}_i^{(t-1)} = \Psi^T\widehat{x}^{(t-1)}$
5: Compute a solution of Equation (9)
   $\widehat{x}^{(t)} = \triangle(y, \Phi, W^{(t)}, \epsilon)$
6: Update $\gamma^{(t)} = \max(\beta\gamma^{(t-1)}, \sigma_c)$
7: Update $\rho = \|\widehat{x}^{(t)} - \widehat{x}^{(t-1)}\|_2 / \|\widehat{x}^{(t-1)}\|_2$
8: $t \leftarrow t + 1$
9: **end while**
10: **return** $\widehat{x}$

Using this scheme, a weighted l_1 problem is solved, and its solution is used as the warm start initialization for the next l_1 iteration that is closer to the l_0 problem. This process is repeated until the solution becomes stationary. A rate parameter β, with $0 < \beta < 1$, is used to control the sequence $\gamma^{(t)}$ such that as $\gamma^{(t)} \to 0$, $t \to \infty$. The value of $\gamma^{(t)}$ should ideally decrease to zero, but in the presence of noise it is set to a lower bound so that $\gamma^{(t)} \geq \sigma_c$. Initially, $\hat{x}^{(0)}$ is set as the solution of the l_1 problem and hence, $\gamma^0 = \sigma_s(\Psi^T \hat{x}^{(t)})$, where $\sigma_s(\cdot)$ stands for the empirical standard deviation of the signal. The re-weighted process continues until the relative variation between successive solutions, $\|\widehat{x}^{(t)} - \widehat{x}^{(t-1)}\|_2 / \|\widehat{x}^{(t)}\|_2$, becomes smaller than the bound η, with $0 < \eta < 1$, or it reaches the maximum number of allowed iterations, $N_{\max}$.

3. SIMULATIONS RESULTS FOR THE PROPOSED TECHNIQUE

In this section, the implementation of the proposed technique is accomplished through the use of a simplified breast phantom. The proposed algorithm is used to detect the presence of tumor tissues from the normal breast tissues. The difference in dielectric contrast between the normal and the malignant tissues is the key for MWI. The dielectric values normally reported for different breast tissues are shown in Table 1. An inverse scattering problem has to be solved to retrieve the dielectric properties of breast tissues from the measured scattered fields. Simulations are conducted on a breast phantom having circular geometry with a 5 mm thick outer skin layer and an inner layer of fatty breast tissues of radius 45 mm. Two tumors of size 6 mm and two glandular inclusions of size 10 mm are eccentrically embedded in the phantom as shown in Fig. 2.

Table 1. Electromagnetic parameters of breast phantom.

Breast profile [27, 28]	Relative permittivity	Conductivity (S/m)
Skin	32	4.0
Fatty breast tissue	9	0.40
Glandular tissue	11	0.45
Tumor	40	4.0

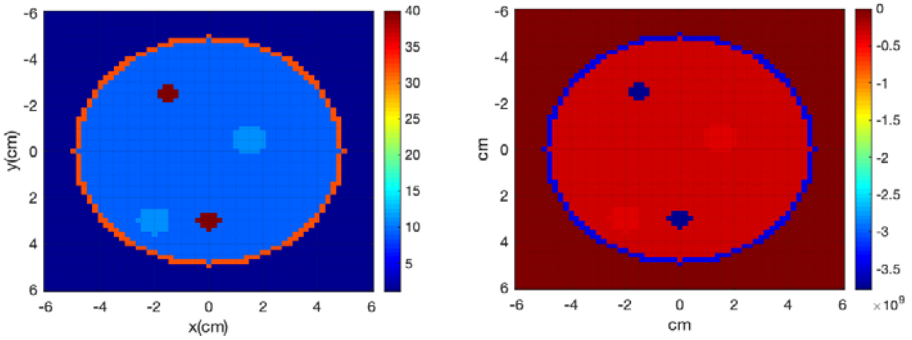

Figure 2. Representation of (a) the permittivity profile ϵ', (b) the conductivity profile ϵ'' of the breast phantom at 3 GHz.

Method of Moments (MoM) is applied to simulate the reflected and scattered waves from various layers of the breast phantom. In this simulation, antennas are assumed to be on the circumference of a circle (as shown in Fig. 1) of radius 12 cm, with the center of the circle coinciding with the centre of the object to be scanned. A set of $N_t = 32$ transmitter antennas are used to excite the breast phantom, and a set of $N_r = 32$ receiver antennas are assumed to collect the back scattered fields. The object

to be imaged is confined within a square domain of size 10 cm and is excited with a Gaussian pulse of frequency ranging from 3 GHz to 4 GHz. By solving the forward problem, the back-scattered fields are generated with a size of $N_t \times N_r$. The simulation is then repeated for L number of frequencies. Hence, the total size of the scattered data is $L \times N_t \times N_r$. The number of discrete frequency points used for excitation is chosen as $L = 20$. This data is given as the input to the proposed RwBP algorithm. The algorithm uses Haar wavelet for the sparse transformation, and the values of error limit and rate parameter are selected as $\eta = 10^{-3}$ and $\beta = 10^{-1}$.

In the ideal scenario, the RwBP algorithm works on the scattered data and produces perfectly reconstructed images which exactly match the input profile. However, in a real-time scenario, random events such as discrete nature of radiation, variation in detector sensitivity, faults in the measuring device, environmental errors (due to factors like stray magnetic fields, vibration, etc.), and errors introduced by the experimenter are always present, and hence, its effect has to be considered. Usually an additive Gaussian noise is added to simulate such kinds of noise, and hence a 30 dB Gaussian noise has been added to the scattered data before inverse profiling [21]. The reconstructed images thereby obtained are shown in Figs. 3(a) & (b). The figure clearly shows that RwBP is able to detect both the tumours and the glandular inclusions correctly.

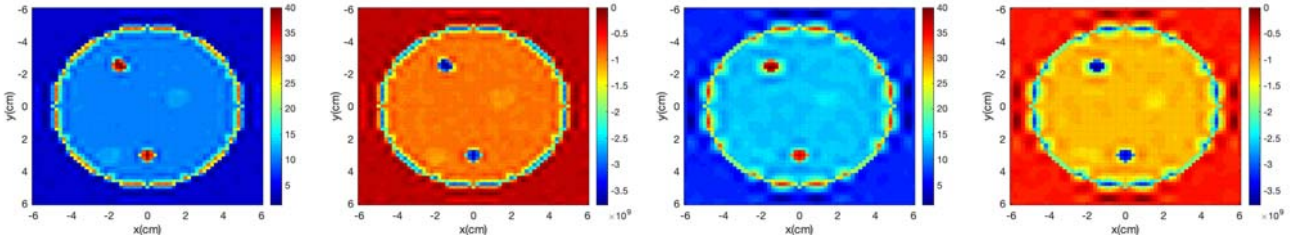

(a) real part-RwBP (b) imaginary part-RwBP (c) real part-TV Regularization (d) imaginary part-TV norm

Figure 3. (a) The permittivity profile ϵ' and (b) the conductivity profile ϵ'' using RwBP method and (c) the permittivity profile ϵ' and (d) the conductivity profile ϵ'' using TV regularization method.

For a fair comparison, the results of the proposed method are compared with the profile reconstructed by Total Variation regularization method (TV norm) [19]. Figs. 3(c) & (d) show the reconstructed profile in the presence of 30 dB noise. It can be noted from Fig. 3 that both the methods are able to detect the tumors as well as fibro-glandular inclusions. The proposed technique is visibly seen to have a a better edge than TV regularisation. To precisely evaluate both the techniques, the Root Mean Square Error (RMSE) is computed and compared. Table 2 shows the RMSE values evaluated for the proposed method and the method described in [19] in the frequency range of 3–4 GHz. The dielectric and conductivity values of the tumor tissues have been reconstructed with a higher accuracy by RwBP as compared to TV norm. Additionally, RwBP is able to reconstruct the fibroglandular inclusions clearly whereas TV norm fails to do so (as seen in Fig. 3). This is because TV regularization produces

Table 2. RMSE value of the reconstructed profiles for TV regularization method and the Re-weighted Basic Pursuit method.

Breast Model	Method	Relative permitivity ϵ	RMSE	Conductivity σ	RMSE
Tumor	TV regularization	39.15	0.850	3.71	0.290
$\epsilon = 40, \sigma = 4.0$	RwBP	39.29	0.710	4.31	0.310
Breast tissue	TV regularization	7.53	1.470	0.318	0.085
$\epsilon = 09, \sigma = 0.40$	RwBP	8.35	0.650	0.427	0.027
Glandular tissue	TV regularization	09.63	1.370	0.329	0.121
$\epsilon = 11, \sigma = 0.045$	RwBP	10.31	0.690	0.424	0.026

Table 3. Accuracy of localization and size estimation for TV regularization method and the Re-weighted Basic Pursuit method.

Breast Model (x, y)	Method	Centroid of Inclusions (x, y) in (mm)	RMSE	Estimated diameter (mm)	Error
Tumor A	TV regularization	$(-0.32, 3.12)$	0.408	6.27	0.27
$(0.0, 3.0)$	RwBP	$(-0.32, 2.95)$	0.401	5.94	-0.06
Tumor B	TV regularization	$(1.41, -2.62)$	0.487	5.78	-0.22
$(1.5, -2.5)$	RwBP	$(1.43, -2.62)$	0.476	5.93	-0.07
Glandular tissue A	TV regularization	$(1.94, 3.14)$	0.199	5.54	4.46
$(2.0, 3.0)$	RwBP	$(2.08, 3.12)$	0.217	9.64	0.36
Glandular tissue B	TV regularization	$(-1.43, -0.61)$	2.18	12.18	0.121
$(-1.5, -0.5)$	RwBP	$(-1.45, -0.43)$	0.165	9.48	0.52

an over-smoothness at the edges and blurs them, which in turn gives an over-estimate of the size of the given object [29] and makes it harder to differentiate the boundary between different types of tissues. The proposed method preserves these sharp edges, and hence the fibro-glandular tissues with a smaller difference in the contrast value can be easily identified even in the presence of noise. Furthermore, from Table 3, another point observed is that the diameters of the reconstructed inclusions in the case of TV norm are larger and result in the extension of the tumors and fibro-glandular inclusions to sizes much larger than that of the input profile. The better tumor localization produced by RwBP that combines the sparsity approach with the weighted minimization verifies the feasibility of the proposed method.

In addition to the above analysis, the effect of noise on the reconstruction produced by both the methods is analyzed and plotted in Fig. 4. From the figure, it can be inferred that for all noise levels, the proposed technique produces a better reconstruction quality as compared to [19]. When the noise level is increased to 25 dB, the proposed technique has a maximum reduction in error as compared to TV norm with an RMSE value of only 0.083 as against 0.32 in the case of TV norm. Thereafter, the difference in error gradually decreases when noise is further increased to 20 dB.

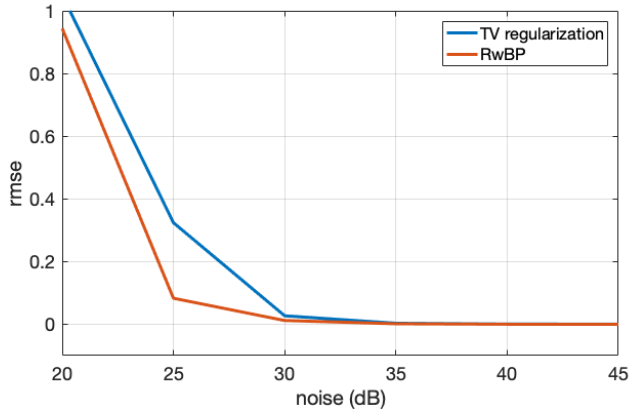

Figure 4. RMSE (%) of the reconstructed profile for different noise levels.

To study the effect of varying levels of noise on the convergence produced by the algorithm, the RMSE has been plotted against the number of iterations in Fig. 5 for different noise levels from 25–40 dB in steps of 5 dB. The algorithm iterates until there is no significant variation between the current and the previous dielectric values. From the figure, it can be inferred that for SNR levels of 25 dB or higher, the solution converges within 12 iterations, and an optimal object profile is reconstructed with an acceptable amount of error. Noise levels as high as 25 dB do not pose a challenge for RwBP to

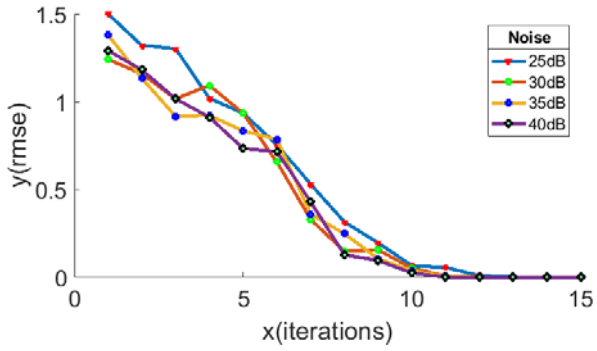

Figure 5. Convergence characteristics.

arrive at the solution. However, it was also observed that when the noise level was increased to 20 dB, the process got stuck at some local minima, and it diverged without giving the desired result after 5 iterations were completed.

This preliminary theoretical analysis suggests that the RwBP algorithm offers better-reconstructed images with few artifacts in the background and small errors in the inner structures of the breast phantom even at noise levels as high as 30 dB. The simulation results obtained were thereafter validated using an experimental study which is discussed in Section 3.1.

3.1. Experimental Validation

In this section, the proposed technique is validated experimentally on a cylindrical phantom. Measurements were conducted inside an anechoic chamber in order to avoid excessive reflection from the environment. The schematic of the measurement setup is shown in Fig. 6(a). The current setup consists of both transmitter and receiver antennas in a multi-static arrangement, a network analyser, a turntable, and a personal computer to remotely control the measurement procedure. The computer coordinates the motion of the stepper motor and the process of data acquisition from each transmitter position. The transmitting antenna used to illuminate the phantom is a standard horn antenna operating in the frequency range 2 GHz to 18 GHz. The receiver antenna used here is an egg-shaped UWB antenna reported in [31]. To achieve a multi-static arrangement, a single receiver antenna is rotated and is successively placed at 36 positions around the object during the experiment. In this way, a mono-static arrangement can be utilised to perform a multi-static imaging procedure.

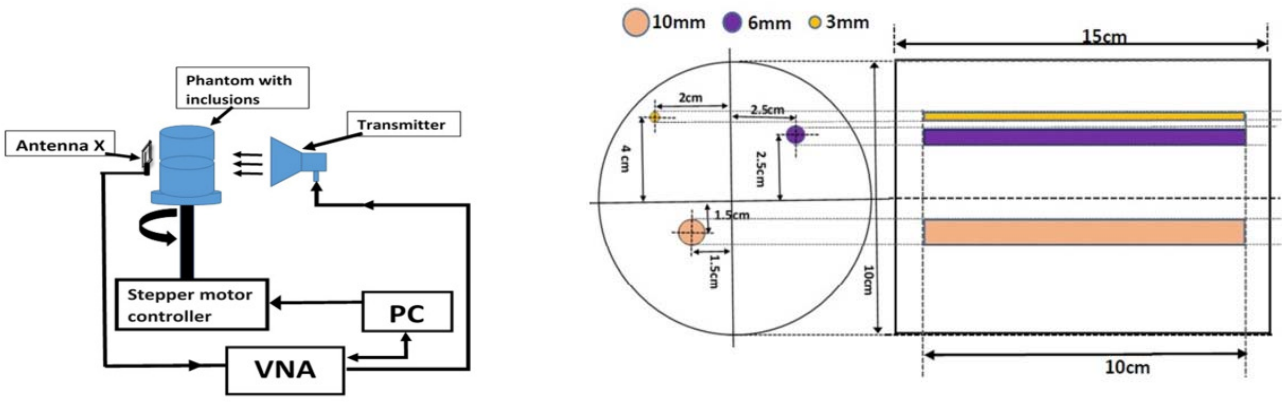

Figure 6. Experimental setup. (a) Flow diagram of the experimental setup. (b) Radial cross section and axial cross section of the cylindrical phantom with dimensions.

Imaging is performed on a phantom with a cylindrical geometry made of Delrin (®Dupont) with a relative permittivity of ($\epsilon_r = 3.7$). Three inclusions of diameters 10 mm, 6 mm, and 3 mm made of PVC ($\epsilon_r = 4.8$) are embedded in the phantom as shown in Fig. 6(b). Materials for phantom and inclusions are selected on the basis of local availability, manufacturing facilities, and sufficient dielectric contrast to mimic early stage malignancies. The materials selected have stable dielectric permittivity over time. The inclusions are eccentrically placed at random radial distances. The total length of the solid cylinder is 15 cm, and the inclusions in their respective radial positions are of height 10 cm.

The egg-shaped antenna used as the receiver is designed to operate in the UWB band and is fabricated on an FR4 substrate. The measured impedance bandwidth of the antenna is from 3.06 GHz to 20 GHz. The antenna is excited with a UWB pulse of the form $V(t) = V_0(t - t_0)e^{(t-t_0)^2/r^2}$ [30]. The cylindrical phantom is mounted on a rotating turn-table controlled by a DC stepper motor. For a particular illumination angle of the transmitting antenna, one total rotation of the turn table is performed with measurements at 36 receiver points (M) with 10 degree angular separation. Proximity of the receiver antenna and its form factor for positioning the antenna at close angles around the specimen are critical to the measurement. The PNAE 8362B Agilent Network Analyser is used to measure the complex transmission parameter S_{21} (dB) in the UWB band at 201 discrete frequency points in the frequency band of 3 GHz to 12 GHz.

Experimental scattered data available in [31], in the range of 3 GHz to 4 GHz, are used to perform the reconstruction process. The reconstruction is done for 20 discrete frequencies. Image reconstruction of the dielectric profile of the phantom was carried out using the proposed method that combines DBIM algorithm and the proposed RwBP technique with a resolution of 61 × 61 pixels. The reconstructed images for various frequencies from 3 GHz to 4 GHz were accumulated to produce the final cross section of the phantom as shown in Fig. 7(a). These results are compared to the reconstruction results reported in [31] (Fig. 7(b)). In the previous work reported in [31], the inclusions of 10 mm and 6 mm diameters were only localized in the reconstructed images, while the inclusion of 3 mm was not discernible. On the other hand, when the reconstruction is performed using the proposed method, it is noted that all the three inclusions are localized, and the relative sizes of the inclusions can be determined as well. Table 4 shows the accuracy of localization for the proposed method, and it is compared with the

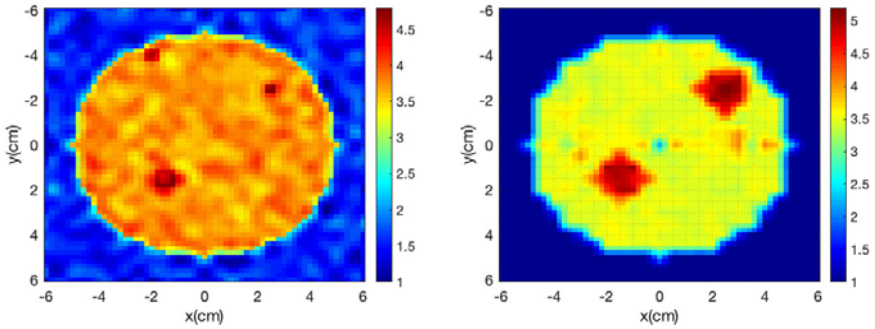

(a) RwBP (b) [30]

Figure 7. The reconstructed object profile in (a) RwBP method and using (b) [31].

Table 4. Comparison of localization and estimated diameter using Re-weighted Basic Pursuit and the method proposed in [31].

Breast Model	Inclusion 1, diameter = 10 mm			Inclusion 2, diameter = 6 mm			Inclusion 3, diameter = 3 mm		
	Location $(-1.5, -1.5)$	Error	estimated diameter	Location $(2.5, 2.5)$	Error	estimated diameter	Location $(-2, 4)$	Error	estimated diameter
RwBP	(-1.505,-1.515)	0.1118	8.32	(2.48, 2.50)	0.0141	3.8	$(-1.97, 4.012)$	0.0228	1.9
Ref. [31]	$(-1.515, -1.525)$	1.67	13.4	(2.453, 2.451)	1.93	12.4	Not detected	Nil	Nil

method proposed in [31]. The improved tumor localization as compared to [31] verifies the feasibility of the proposed method.

4. CONCLUSION

A quantitative method for reconstructing the dielectric contrast profile of the scatterer in a breast imaging setup is proposed and implemented using the compressive sensing framework. The proposed method combines the DBIM with the Re-weighted Basic Pursuit algorithm for solving the inverse ill-posed problem. The proposed method is able to extract the quantitative information about the size, shape, location, and dielectric profiling of the tissue inclusions using an iterative reconstruction framework within microwave tomography. The method produces a significant reduction in the reconstruction error as compared to the TV norm method with an RMSE value of only 0.083 as against 0.32 in the case of TV norm in the presence of 25 dB noise. The technique was validated experimentally, and it was observed that for the object profile used for imaging, all the three inclusions were localized, and the relative sizes of the inclusions were determined as well. Accuracy in estimating the quantitative information like localization, size, and shape was high compared with previously published works.

ACKNOWLEDGMENT

The authors are thankful to Prof. P. Mohanan and research scholar, Manoj Mani, at the Centre for Research in Electromagnetics and Antennas (CREMA) at Cochin University of Science and Technology for the experimental facilities extended towards the completion of this work.

REFERENCES

1. Semenov, S. Y., A. E. Bulyshev, V. G. Posukh, Y. E. Sizov, T. C. Williams, and A. E. Souvorov, "Microwave tomography for detection/imaging of myocardial infarction. 1. Excised canine hearts," *Ann. Biomed. Eng.*, Vol. 31, 262–270, 2003, DOI: 10.1114/1.1553452.
2. Anishchenko, L. N., I. L. Alborova, M. A. Chizh, and A. V. Zhuravlev, "Microwave imaging of biological tissue phantom in different frequency ranges," *2016 Progress In Electromagnetic Research Symposium (PIERS)*, 4639–4643, Shanghai, China, August 8–11, 2016.
3. Yaswanth, K., S. Bhattacharya, and U. K. Khankhoje, "Algebraic reconstruction techniques for inverse imaging," *2016 International Conference on Electromagnetics in Advanced Applications (ICEAA)*, Cairns, Australia, September 2016.
4. Benny, R., T. A. Anjit, and P. Mythili, "An overview of microwave imaging for breast tumor detection," *Progress In Electromagnetics Research B*, Vol. 87, 61–91, 2020.
5. Huang, T. and A. S. Mohan, "Microwave imaging of perfect electrically conducting cylinder by micro-genetic algorithm," *IEEE Antennas and Propagation Society Symposium*, Vol. 1, IEEE, 2004.
6. Semenov, S. Y., et al., "Microwave-tomographic imaging of the high dielectric-contrast objects using different image-reconstruction approaches," *IEEE Trans. Microw. Theory Tech.*, Vol. 53, No. 7, 2284–2294, July 2005.
7. Chew, W. C. and G. P. Otto, "Microwave imaging of multiple metallic cylinders using shape functions," *IEEE Antennas and Propagation Society International Symposium, 1992 Digest*, IEEE, 1992.
8. Colgan, T. J., S. C. Hagness, and B. D. van Veen, "A 3-D level set method for microwave breast imaging," *IEEE Trans. Biomed. Eng.*, Vol. 62, No. 10, 2526–2534, 2015.
9. Bayat, N. and P. Mojabi, "A mathematical framework to analyze the achievable resolution from microwave tomography," *IEEE Trans. Antennas and Propag.*, Vol. 64, No. 4, 1484–1489, 2016.
10. Rocca, P., M. Benedetti, M. Donelli, D. Franceschini, and A. Massa, "Evolutionary optimization as applied to inverse problems," *Inverse Prob.*, Vol. 25, 1–41, 2009.
11. Majobi, P. and J. LeVetri, "Comparison of TE and TM inversions in the framework of the GaussNewton method," *IEEE Trans. Antennas and Propag.*, Vol. 64, 1336–1348, 2010.

12. Candès, E. J. and M. B. Wakin, "An introduction to compressive sampling," *IEEE Signal Processing Magazine*, Vol. 25, No. 2, 21–30, 2008.
13. Lustig, M., D. Donoho, and J. M. Pauly, "Sparse MRI: The application of compressed sensing for rapid MR imaging," *Magnetic Resonance in Medicine*, Vol. 58, No. 6, 1182–1195, 2008.
14. Pan, X. and E. Y. Sidky, "Image reconstruction in circular cone-beam computed tomography by constrained, total-variation minimization," *Physics in Medicine and Biology*, Vol. 53, No. 17, 4777–4807, 2008.
15. Chinn, G., P. D. Olcott, and C. S. Levin, "Sparse signal recovery methods for multiplexing PET detector readout," *IEEE Transactions on Medical Imaging*, Vol. 32, 932–942, 2013.
16. Rudin, L. I. and S. Osher, "Total variation based image restoration with free local constraints," *Proc. International Conf. Image Processing*, Austin, USA, 1994.
17. Zhou, H. and R. M. Narayan, "Microwave imaging of nonsparse object using dual-mesh method and iterative method," *IEEE Trans. Antennas and Propag.*, Vol. 67, 504–512, 2019.
18. Yalcin, E. and O. Ozdemir, "Sparsity based regularization for microwave imaging with NESTA algorithm," *Proc. IEEE Conference on Antennas Measurements and Applications (CAMA)*, Tsukuba, Japan, 2017.
19. Jamali, N. H., et al., "Image reconstruction based on combination of inverse scattering technique and total variation regularization method," *Indonesian Journal of Electrical Engineering and Computer Science*, Vol. 5, No. 3, 569–576, 2017.
20. Chen, S. and D. Donoho, "Basis pursuit," Technical Report, Department of Statistics, Stanford University, 1995.
21. Azghani, M. and F. Marvasti, "L2-regularized iterative weighted algorithm for inverse scattering," *IEEE Trans. Antennas and Propag.*, Vol. 64, No. 6, 2293–2300, 2016.
22. Tibshirani, R., "Regression shrinkage and selection via the LASSO," *J. Roy. Statist. Soc.*, ser. B, Vol. 58, No. 1, 267–288, 1996.
23. Chartrand, R. and V. Staneva, "Restricted isometry properties and nonconvex compressive sensing," *Inverse Prob.*, Vol. 24, 035020, 2008.
24. Wang, Y., J. Zeng, Z. Peng, X. Chang, and Z. Xu, "Linear convergence of adaptively iterative thresholding algorithms for compressed sensing," *IEEE Transactions on Signal Processing*, Vol. 63, No. 11, 2957–2971, June 2015.
25. Mansour, H. and O. Yilmaz, "Support driven reweighted 1 minimization," *2012 IEEE International Conference on Acoustics Speech and Signal Processing (ICASSP)*, 2012.
26. Asif, M. S. and J. Romberg, "Sparse recovery of streaming signals using l_1-homotopy," *IEEE Transactions on Signal Processing*, Vol. 62, No. 16, 4209–4223, July 2014.
27. Tavassolian, N., H. Kanj, and M. Popovic, "Assessment of Dark eyes antenna radiation in the vicinity of the realistic breast model," *12th International Symposium on Antenna Technology and Applied Electromagnetics (ANTEM)*, Montreal, Canada, July 2006.
28. Fear, E. C. and M. Okoniewski, "Confocal microwave imaging for breast tumor detection: Application to a hemispherical breast model," *2002 IEEE MTT-S International Microwave Symposium Digest*, Vol. 3, 1759–1762, June 2–7, 2002.
29. Estatico, C., M. Pastorino, and A. Randazzo, "A novel microwave imaging approach based on regularization in banach spaces," *IEEE Trans. Antennas and Propag.*, Vol. 60, No. 7, 3373–3381, 2012.
30. Fear, E. C., X. Li, S. C. Hagness, and M. A. Stuchly, "Confocal microwave imaging for breast cancer detection: Localization of tumors in three dimensions," *IEEE Trans. Biomed. Eng.*, Vol. 49, No. 8, 812–822, 2002.
31. Philip, C., T. A. Anjit, and P. Mythili, "A compact egg-shaped UWB antenna for breast dielectric profile imaging," *International Journal of Scientific & Technology Research (IJSTR)*, Vol. 9, No. 3, March 2020.